ESC European Society of Cardiology

Cardiovascular Research (2021) **117**, 2652–2663
doi:10.1093/cvr/cvab074

Targeted delivery of protein arginine deiminase-4 inhibitors to limit arterial intimal NETosis and preserve endothelial integrity

Roberto Molinaro [1,2†], Mikyung Yu [3†], Grasiele Sausen [1], Colette A. Bichsel[4], Claudia Corbo [3,5], Eduardo J. Folco [1], Gha Young Lee [3], Yuan Liu[3], Yevgenia Tesmenitsky[1], Eugenia Shvartz[1], Galina K. Sukhova [1], Frederik Kloss [1], Kevin J. Croce[1], Omid C. Farokhzad[3], Jinjun Shi[3*‡], and Peter Libby [1*‡]

[1]Division of Cardiovascular Medicine, Department of Medicine, Brigham and Women's Hospital, Harvard Medical School, 77 Avenue Louis Pasteur, Boston, MA 02115, USA; [2]Business Development of Research, IRCCS San Raffaele Hospital, Milan, Italy; [3]Center for Nanomedicine and Department of Anesthesiology, Brigham and Women's Hospital, Harvard Medical School, Boston, MA 02115, USA; [4]Department of Surgery, Vascular Biology Program, Boston Children's Hospital, Harvard Medical School, Boston, MA, USA; and [5]Department of Medicine and Surgery, Nanomedicine Center NANOMIB, University of Milano-Bicocca, Milano, Italy

Received 20 December 2019; editorial decision 1 February 2021; accepted 3 March 2021; online publish-ahead-of-print 5 March 2021

Time for primary review: 32 days

Aims Recent evidence suggests that 'vulnerable plaques', which have received intense attention as underlying mechanism of acute coronary syndromes over the decades, actually rarely rupture and cause clinical events. Superficial plaque erosion has emerged as a growing cause of residual thrombotic complications of atherosclerosis in an era of increased preventive measures including lipid lowering, antihypertensive therapy, and smoking cessation. The mechanisms of plaque erosion remain poorly understood, and we currently lack validated effective diagnostics or therapeutics for superficial erosion. Eroded plaques have a rich extracellular matrix, an intact fibrous cap, sparse lipid, and few mononuclear cells, but do harbour neutrophil extracellular traps (NETs). We recently reported that NETs amplify and propagate the endothelial damage at the site of arterial lesions that recapitulate superficial erosion in mice. We showed that genetic loss of protein arginine deiminase (PAD)-4 function inhibited NETosis and preserved endothelial integrity. The current study used systemic administration of targeted nanoparticles to deliver an agent that limits NETs formation to probe mechanisms of and demonstrate a novel therapeutic approach to plaque erosion that limits endothelial damage.

Methods and results We developed Collagen IV-targeted nanoparticles (Col IV NP) to deliver PAD4 inhibitors selectively to regions of endothelial cell sloughing and collagen IV-rich basement membrane exposure. We assessed the binding capability of the targeting ligand *in vitro* and evaluated Col IV NP targeting to areas of denuded endothelium *in vivo* in a mouse preparation that recapitulates features of superficial erosion. Delivery of the PAD4 inhibitor GSK484 reduced NET accumulation at sites of intimal injury and preserved endothelial continuity.

Conclusions NPs directed to Col IV show selective uptake and delivery of their payload to experimentally eroded regions, illustrating their translational potential. Our results further support the role of PAD4 and NETs in superficial erosion.

* Corresponding authors. Tel: +1 617 525 4383; fax: +1 617 525 4400, E-mail: plibby@bwh.harvard.edu (P.L.); Tel: +1-617-525-8798, E-mail: jshi@bwh.harvard.edu (J.S.)

† The first two authors contributed equally to this manuscript.

‡ The last two authors contributed equally to this manuscript.

Graphical Abstract

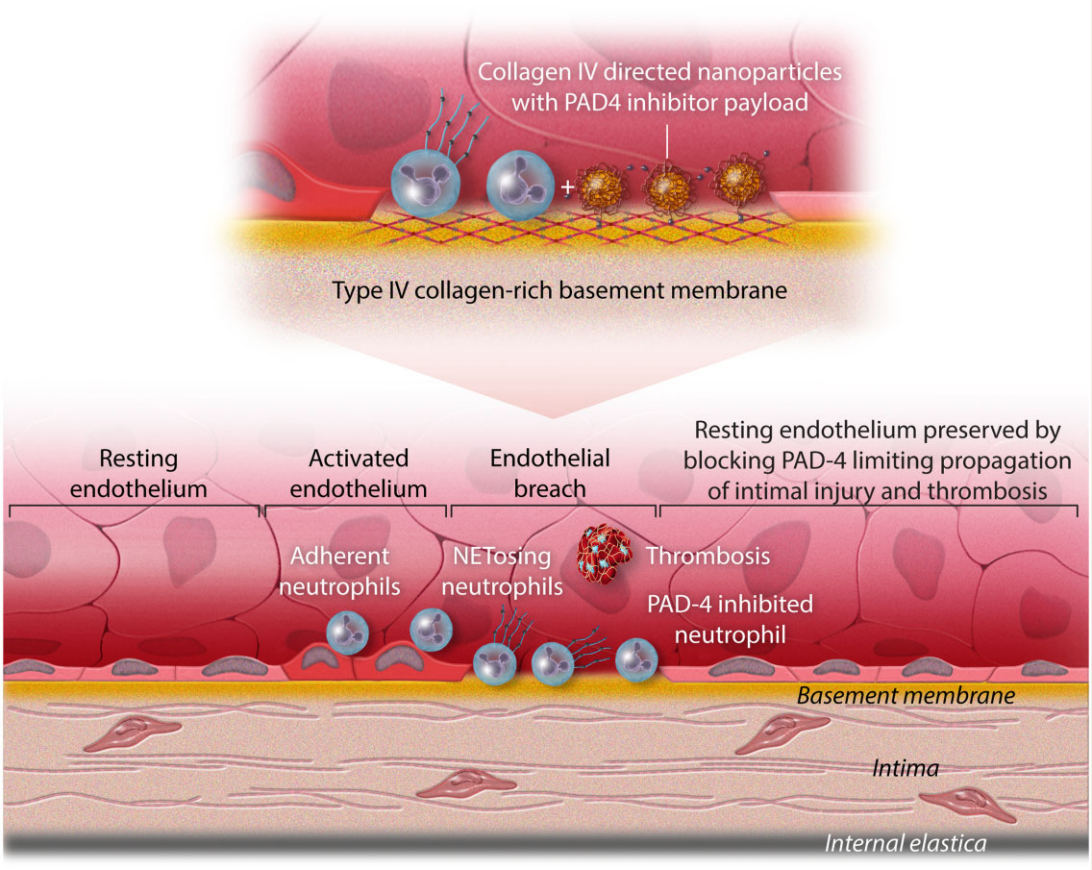

Keywords Atherosclerosis • Experimental superficial erosion • Cardiovascular nanomedicine • Targeted nanoparticles • Neutrophil extracellular traps

Breaches in the endothelial monolayer can provoke arterial thromboses, particularly those precipitated by superficial erosion. Desquamation of endothelial cells (ECs) uncovers the basement membrane, a subendothelial structure rich in type IV collagen. Activated ECs (denoted here by the transition from a squamous morphology to a more columnar morphology) express adhesion molecules that can bind cognate ligands on blood leukocytes and recruit them to the intimal surface. Polymorphonuclear leucocytes can undergo a specialized form of cell death [neutrophil extracellular trap (NET) formation] which involves the extrusion of strands of DNA decorated with the neutrophil granular constituents such as myeloperoxidase (a generator of the pro-oxidant species hypochlorous acid) and also bind other proteins such as tissue factor procoagulant. This study used nanoparticles that selectively target type IV collagen, due to a peptide ligand, that home to areas of endothelial denudation. These nanoparticles can carry a payload of inhibitor of the enzyme protein arginine deiminase (PAD)-4, involved in NET formation. Delivery of these targeted nanoparticles carrying the PAD-4 inhibitor to areas of endothelial activation reduced NET formation and preserved intimal integrity and endothelial barrier function. This approach has both diagnostic and therapeutic potential for delineating and treating zones of superficial erosion. As acute coronary syndromes due to superficial erosion may not require urgent coronary revascularization, the development of methods to identify areas of endothelial breaches, and local delivery of therapeutics has translational potential.

Introduction

Despite successes in acute care, lifestyle measures, and pharmacologic treatments, acute coronary syndromes (ACS) remain the leading cause of morbidity and mortality.[1] Although thin-capped fibroatheroma and plaque rupture have received intense attention as substrates for ACS over the decades, more recent evidence showed that such 'vulnerable' plaques actually rarely rupture and cause clinical events; only ~5% of thin-capped plaques provoked ACS during a 3.4-year follow-up period.[1] We have marshalled evidence that superficial plaque erosion has emerged as a growing cause of residual thrombotic complications of atherosclerosis in an era of increased preventive measures including lipid-

lowering, antihypertensive therapy, and smoking cessation.[2] Indeed, contemporary studies using optical coherence tomography to characterize current culprit lesions suggest that superficial erosion has become more prominent, now accounting for about one-third of ACS.[3]

The lesions associated with erosion have areas of denuded endothelium and exposed basement membrane, a rich extracellular matrix, intact fibrous caps, sparse lipid, and few mononuclear cells. Eroded lesions and endothelial apoptosis in human atherosclerotic arteries may localize in regions of disturbed arterial flow.[4] We have implicated neutrophil extracellular traps (NETs) in superficial erosion. NETs form through a programmed cell death pathway sometimes referred to as NETosis.[3] NETs consist of web-like structures derived from decondensed chromatin with histones, proteases, and other proteins which can propagate local thrombosis and activate ECs.[5,6] NETosis often involves the activity of protein arginine deiminase (PAD)-4.[7,8] PAD4 catalyses the conversion of the cationic aminoacid arginine to neutral citrulline, thus interrupting electrostatic interactions between histones and DNA, which results in DNA de-condensation and NET release. We recently reported that the surface of erosion-prone atheromata exhibits more NETs in regions of apoptotic ECs than stable or rupture-prone lesions.[9] Moreover, we found that mice lacking PAD4 showed reduced endothelial injury and preserved barrier function when subjected to experimental conditions designed to recapitulate aspects of superficial erosion. These findings point to the causal participation of PAD4 and NETs in exacerbating the atherothrombotic complications of intimal arterial lesions implicated in superficial erosion.

Nanotechnology offers potent tools for delivering therapeutics to diseased tissue, exploiting the particular features of specific pathological conditions. For example, sites of nascent superficial intimal erosion will uncover patches of the subjacent basement membrane of the arterial intima. Type IV collagen (Col-IV), a non-fibrillar protein, comprises about 50% of the basement membrane matrix. We previously reported the therapeutic capabilities of polymeric nanoparticles (NPs) that target Col-IV, capable of encapsulating and delivering a payload of peptides, proteins, siRNAs, or small-molecule drugs in various settings including advanced atherosclerosis and balloon-injured vasculature.[10–17]

This study tested the hypothesis that Col IV-targeted NPs (Col IV-NPs) can deliver PAD4 inhibitors selectively to regions of EC sloughing and collagen IV-rich basement membrane exposure, and attenuate the amplification, persistence, and propagation of superficial erosion and consequent thrombosis (*Graphical abstract*).

Materials

Poly(d,l-lactide) with terminal ester groups (PLA–OCH_3, inherent viscosity 0.26–0.54 dL g^{-1} in chloroform) was purchased from Durect Lactel Absorbable Polymers (Pelham, AL, USA). DSPE–mPEGs (1,2-distearoyl-sn-glycero-3-phosphoethanolamine-N-[methoxy(polyethylene glycol)]) with 1000 kDa (DSPE–mPEG1000), 1,2-distearoyl-sn-glycero-3-phosphoethanolamine-N-[maleimide(polyethylene glycol)-2000] (DSPE–PEG2000–MAL), 1,2-dilauroyl-sn-glycero-3-phosphocholine (DLPC), 1,2-dioleoyl-sn-glycero-3-phosphoethanolamine-N-(Cyanine 5.5) (18:1 Cy5.5 PE), 1,2-dioleoyl-*sn*-glycero-3-phosphoethanolamine-N-(lissamine rhodamine B sulfonyl) (ammonium salt) (18:1 Liss Rhod PE), were purchased from Avanti Polar Lipids. Cy5.5-NHS monoester was obtained from GE Healthcare Life Sciences. The Collagen type IV (Col IV)-targeting peptide (KLWVLPK[GGGC]) was obtained from Massachusetts Institute of Technology (Biopolymers & Proteomics Core Facility, Koch Institute, USA). Detailed synthesis information is in ref.[15] Immunohistochemical analysis used as secondary antibodies rabbit anti-rat, biotinylated—Vector, cat# BA-4001and goat anti-rabbit, biotinylated—Vector, cat# BA-1000.

Methods

Fluorescently labelled NPs and Col IV-NPs

To investigate the binding capability of the Col IV-NPs or to select an optimal formulation, we prepared fluorescently labelled NP or Col IV-NP formulations. PLA-OCH3 was dissolved in a mixture of ethyl acetate and benzyl alcohol (40 mg/mL). Different molar ratios of DSPE-mPEG1000: DLPC: Col IV-DSPE-PEG2000[15] (70:30-X:X, $X = 0–30$) were prepared by dissolving in a mixture of ethyl acetate and benzyl alcohol (40 mg/mL) at 70% of the PLA weight. After that, 18:1 Cy5.5 PE or 18:1 Liss Rhod PE (0.5 wt% of total polymer/lipid mixture) was added to the solution. The mixture was then added drop-wise into an aqueous solution with gentle stirring and then sonicated with a probe. Free molecules and the remaining organic solvent were removed by washing the NP solution three times using an Amicon Ultra-15 centrifugal filter (EMD Millipore, Darmstadt, Germany), and then resuspended in PBS. The nanoparticle (NP) sizes and ζ-potentials were measured by quasi-electric laser light scattering using a ZetaPALS dynamic light-scattering (DLS) detector (15 mW laser, incident beam ¼ 676 nm; Brookhaven Instruments). The NP diameters measured by DLS were displayed as the effective diameters, which were average of the intensity-, volume-, and number-weighted size distributions, calculated based on the Lognormal distribution. Samples for TEM (JEOL 2011 at 200 kV) were stained with 0.75% uranyl formate or 1% uranyl acetate and measured on a coated copper grid.

Preparation and characterization of GSK484-NPs and Col IV–GSK484–NPs

GSK484 is hydrophobic, necessitating dissolution in solvents such as 99.9% ethanol and injection into mice after dilution in saline.[18] The poor water solubility of GSK484 (GSK) comprises an obstacle for conventional clinical translation. Development of Col IV-NP delivery formulations that encapsulate GSK484 can obviate the solubility issue of the inhibitor, and enables controlled release of GSK484 at target lesions. For the preparation of GSK–NPs and Col IV–GSK–NPs, GSK was dissolved in DMSO (0.85 mg, 80 mg/mL) and added to the PLA/lipid mixture solution. The PLA/lipid/drug mixture in the organic phase was then added into the aqueous solution as above described. Hydrodynamic size, size homogeneity (PDI), and surface charge were analysed by DLS. The amount of drug-loading in the NPs was analysed using high performance liquid chromatography (HPLC).

Drug release kinetics study

NPs were aliquoted into mini-dialysis tubes (Slide-A-Lyzer, MWCO: 10 kDa, ThermoFisher Scientific) that were placed in 50 mL of PBS (pH 7.4) at 37°C. At different time points, NPs in each tube were collected and prepared for HPLC measurement. The remaining drug in NPs at different time points was quantified by HPLC (C18 column: 2.1 × 15 cm, gradient: 0.1–0.1%/20′–100%/80′, A: 0.05% TFA and B: 0.043% TFA, 80% ACN). Experiments were carried out in triplicate.

Cell culture experiments

Human saphenous vein endothelial cell (HSVEC) isolation and culture followed a protocol previously described by our lab and others.[19,20] HSVEC were obtained from saphenous vein segments discarded from coronary artery bypass surgeries as described previously and authorized by the local Human Investigation Research Committee. After flushing out blood cells

with cold HBSS, ECs were harvested by 0.1% collagenase type II digestion (Worthington) of the vein segment and cultured on 1% gelatin-coated dishes in Medium 199 (Lonza) supplemented with 20% foetal bovine serum (FBS), penicillin/streptomycin, L-glutamine, heparin, and 0.05 mg/mL ECGS (Alfa Aesar). We characterized these cultures with Ulex europeaeus lectin and vWf staining. The authors declare that investigation conformed to the principles outlined in the Declaration of Helsinki.

In vitro experiments used HSVECs between passages 2 and 5. For confocal microscopy analysis, glass slides were coated with fibronectin (10 μg/ml) overnight at 4°C. Endothelial colony-forming cells (ECFCs) from umbilical cord blood were cultured on 10 μg/mL fibronectin-coated dishes in EGM2 medium (Lonza) supplemented with an additional 10% FBS. They were transduced with a DsRed lentiviral vector. Human white adipose tissue-derived mesenchymal stem cells (watMSC) were cultured in DMEM with L-glutamine (Sigma) supplemented with 10% FBS and penicillin/streptomycin.

Collagen IV binding studies

To evaluate the optimum amount of the Col IV-directed peptide on the NP surface, we performed binding studies as previously reported.[10] Briefly, 96-well plates were coated with collagen IV (1 μg/mL) overnight at 4°C. Wells were then washed twice with PBS, blocked with 3% BSA for 2 h at room temperature, and incubated for 30 s at 4°C with 100 μL of fluorescently labelled NPs and Col IV-NPs (0.75 μg/ml of fluorescent dye) at different ligand densities (from 1 to 30 wt%). Wells were then washed three times with 100 μL PBS at room temperature. Fluorescence was measured after incubation of each sample with 100 μL DMSO. Results are expressed as fluorescence relative to NPs and represent the mean ± standard deviation (SD) of eight replicates per sample.

Basement membrane adhesion studies

NP adhesion studies were performed under both static (2D) and dynamic (3D) conditions. In the former case, HSVEC were cultured for 72 h to allow them deposit a layer of basement membrane. Cells were then removed with ammonium hydroxide (0.017 M; two incubations of 10 minutes each at room temperature). The remaining basement membrane was then washed, blocked and incubated with either bare or Col IV-NPs as reported above. Data are expressed as the mean ± SD of eight replicates per sample (at least three fields of view per each sample). Cultured HSVECs were previously authenticated by morphology, and the assessment of the expression of von Willebrand Factor by immunofluorescence and QPCR.[21]

Development of 3D microvessel-like tubules *in vitro*

To evaluate NPs' adhesion properties in dynamic conditions, microfluidic chips were fabricated as previously described.[18] Confluent ECFC were prepared in a fibrin solution [5 mg/mL human fibrinogen (Sigma), 1 U/mL human thrombin (Sigma)] at a final concentration of 4×10^6 cells/ml. Immediately after resuspension, they were filled into the central diamond-shaped chamber of the custom-made microfluidic chip (1.5 mm width, 0.1 mm height). WatMSC were separately resuspended in a fibrin gel at a final concentration of 1×10^6 cells/mL and one drop of gel pipetted into the outer reservoirs. After clotting, EGM2 medium (Lonza) was added into the reservoirs, and the chips were incubated at 37°C and 5% CO2. Medium was changed every day, to an alternating filling height (80 μL in one reservoir, 20 μL in the other) between the reservoirs to generate a hydrostatic pressure difference across the gel chamber. After 5 days, the chips were washed once with EBM2 media, perfused with ammonium hydroxide (0.017 M; 20 min at 37°C) or EBM2 (control), washed 3× with EBM2 and subsequently loaded with Col IV-NP (0.75 μg/mL of fluorescent dye; 20 min at 37°C). Chips were then washed, fixed in 4% paraformaldehyde, stained with collagen IV antibody (Abcam) and anti-rabbit alexa-fluor 488 (Invitrogen). Images were taken with a LSM880 confocal microscope (Zeiss).

Animals

All animal experiments were performed in accordance with the guidelines of the Animal Welfare Act and the Guide for the Care and Use of Laboratory Animals approved by the Institutional Animal Care and Use Committee of the Harvard Medical Area Standing Committee on Animals (Protocol #: 2016N000293; PI: Libby, Peter). $ApoE^{-/-}$ male mice (Jackson Laboratories, USA), 6–12 weeks of age, were housed in the Harvard Medical School Facilities at the New Research Building (Boston, MA, USA). $ApoE^{-/-}$ mice consumed a normal chow diet with water ad libitum. Mice were certified free of common pathogens by the suppliers and were monitored by the Harvard Medical Area Standing Committee on Animals. Mice were anaesthetized with 90–200 mg/kg ketamine/10 mg/kg xylazine intraperitoneally. After recovery from anaesthesia, the animals were given a standard diet and water ad libitum. Post-operative analgesia was administered using 0.05–0.1 mg/kg of buprenorphine (first dose prior to animal recovering and second dose at 8–12 h from the first dose for the first day; once the second day). Post-surgical animals were evaluated daily for a minimum period of 4 days as required by the BWH CCM institutional policy.

Flow-mediated superficial erosion

We used an *in vivo* approach to study superficial erosion in mice which replicates features of human eroded lesions.[9,22] First, we crafted intimal lesions that share characteristics of human eroded plaques (low lipid content, a glycosaminoglycan- and proteoglycan rich matrix). For this purpose, eight-week-old $ApoE^{-/-}$ mice underwent electrical current injury of the left common carotid artery (LCCA) using a bipolar microcoagulator (Erbe ICC 200, USA) with a current pulse of 3 W. We then introduced (four weeks later) a calibrated flow disturbance by placing a cone-shaped polyethylene cuff (Proto Labs, USA) around the adventitia of the previously injured LCCA. The flow perturbation promoted EC desquamation and neutrophil recruitment selectively in the EC layer and caused intralumenal thrombosis where the constrictive cuff (CC) was applied to the LCCA. This preparation permits probing of the mechanisms of arterial thrombi in superficial erosion. Flow perturbation was conducted at different time points and mice were euthanized by CO_2 inhalation and bilateral thoracotomy. Mice were then perfused via left ventricular cannulation with cold PBS, and then fixed with 4% paraformaldehyde (PFA). Distal and proximal LCCA samples were collected and embedded in optimal cutting temperature medium. For immunohistochemical/immunofluorescence investigation, 6 μm cryosections were prepared and stained. For en face microscopy experiments, carotid arteries were perfused as described above followed by a fixation with cold 4% PFA. They were then dissected and opened longitudinally on a Sylgard dish and fixed in 4% PFA for 48–72 h. Fixation was quenched with 100 mM glycine (pH 7.4).

Immunohistochemistry/immunofluorescence and endothelial permeability analysis

Immunostaining of frozen cross-sections used a rat monoclonal anti-mouse Ly6G (clone 1A8), a rabbit polyclonal anti-citrullinated Histone H3 (H3cit, Abcam), a rat monoclonal anti-CD31 (BD Pharmingen), or a rabbit polyclonal anti-collagen IV (anti-Col IV, Abcam). Immunostaining was amplified using peroxidase-conjugated streptavidin complexes (Vector Laboratories), and peroxidase was detected using AEC (Vector Laboratories) substrate. Sections were lightly counterstained with haematoxylin, mounted in gelatin glycerol, and examined with a bright field microscope (Nikon Optiphot-2 equipped with a Nikon digital camera DXM 1200F). For double immunofluorescence studies, cross sections were incubated with primary antibodies followed by incubation with fluorophore-coupled anti-species antibody (Life Technologies), stained with DAPI, and mounted with fluorescent mounting medium (DAKO). Slides were kept in the dark at 4°C. Downstream NET burden was quantified by measuring the area of H3 staining within the luminal surface normalized for intima area. Endothelial continuity is expressed as percentage of CD31 staining within the luminal area.

Endothelial permeability was assessed *in vivo* by an Evans Blue dye (EBD, Sigma) extravasation assay as previously reported.[9] Briefly, we retro-orbitally injected EBD (50 µL, 7% EBD in PBS) at 24 after the last treatment administration. After 10 min from EBD injection, we euthanized, perfused and fixed mice ($n = 5–8$) as above reported. LCCA were harvested by longitudinal opening from the aortic arch to the bifurcation and stabilized on glass with hardening mounting medium (Vector, Vecta Mount H-5000). Carotids were examined by bright field imaging.

In vivo biodistribution

ApoE$^{-/-}$ mice ($n = 3$) that underwent superficial erosion procedure as described above were injected with the rhodamine labelled NPs or Col IV–NPs at 1 h after CC placement and sacrificed at 24 h post-injection. After perfusion, both carotids were collected and visualized using the fluorescence reflectance imaging (FRI) system (Kodak Image-Station 4000, Carestream Health, Rochester, NY, USA). The fluorescence intensities from the NPs (lissamine rhodamine B; excitation/emission 560 nm/583 nm) were quantified following manufacturer's instructions. The values are represented as relative fluorescence units. For drug accumulation studies, Cy5.5 (excitation/emission 675 nm/720 nm) was loaded into both NPs and Col IV-NPs to mimic GSK. NPs were injected in PBS as vehicle. Briefly, ApoE$^{-/-}$ mice ($n = 3–5$) that underwent the superficial erosion procedure received cy5.5-loaded NPs or Col IV–NPs at 1 h after CC placement and sacrificed at 4 and 24 h post-injection. Cy5.5 accumulation downstream and upstream to the site of flow perturbation was evaluated through FRI analysis on carotids collected as described above.

In vivo evaluation of the therapeutic efficacy of GSK484

ApoE$^{-/-}$ mice ($n = 8–12$ per group) underwent superficial erosion procedure as described above and previously reported.[9,22] At 1 h after CC placement, GSK (4 mg/kg) was administered either once per day for 7 days or three times in 7 days either free or encapsulated into NPs, respectively. At 7 days, mice were sacrificed and perfused as above described. Carotids were then harvested and embedded in OCT blocks, which were immediately frozen at -80°C. GSK treatment effects were evaluated by the ability to reduce NET accumulation and to preserve endothelial continuity at the site of flow perturbation.

Statistical analysis

Animals were randomly allocated to treatment or control groups. Investigators were blinded to the group allocation during both the experiment and image analysis. Data were analysed to assess normality of distribution. Data are expressed as mean ± SD and analysed by one-way analysis of variance (ANOVA) as appropriate for multiple comparisons. *P*-values were calculated using the Student's *t*-test or one-way ANOVA with *post hoc* Tukey analysis for normally distributed data. For non-normally distributed data, the Mann–Whitney rank sum test was used. A $P < 0.05$ was considered statistically significant.

Results

Synthesis and characterization of Col IV-targeted nanoparticles

We recently described the development and physicochemical properties of Col IV-NPs, as well as their biological features in a mouse setting of advanced atherosclerosis.[15] In particular, the targeting of these lipid-polymer hybrid NPs depends on the length of polyethylene glycol (PEG) coating molecules on the NPs relative to the ligand linker.[15] Using this formulation strategy, we prepared Col IV-NPs composed of poly (D, L-lactide) (PLA) as a core and PEGylated phospholipid layer (DSPE-PEG1000/DLPC/Col IV-DSPE-PEG2000) as a shell. We then tuned ligand density to optimize Col IV-NPs by changing the molar ratio of Col IV-DSPE-PEG2000 from 1% to 30% (Supplementary material online, *Figure S1*). We assessed the binding capabilities of the targeting ligand to Col IV-coated wells as previously reported.[10] Evaluation of binding properties of Col IV-NPs at different heptapeptide densities to Col IV-coated wells revealed that a ligand density of 15% had the highest binding affinity (Supplementary material online, *Figure S1*). Further experiments used these optimized NP. Next, we tested *in vitro* NP adhesion to a basement membrane deposited by primary HSVECs previously seeded on a fibronectin-coated glass slide (see Methods section) under both static (2D) and dynamic (3D) conditions. When compared to bare NPs, Col IV-NPs showed a 40-fold increased adhesion to the EC-derived basement membrane (*Figure 1A and B*). Experiments with a microfluidic chip containing perfusable blood vessel-like tubular structures extended these findings to a 3D configuration. These structures consist of ECs, supported by perivascular mesenchymal cells, that self-assemble inside the chip within 5 days, as previously described.[23] The endothelial monolayer forms adherens and tight junctions, as demonstrated by immunostaining for vascular endothelial-cadherin and platelet EC adhesion molecule-1/CD31 and Zona Occludens 1, while Col IV staining indicated secreted basement membrane components on the basolateral aspect of the microtubules.[23] Dynamic perfusion of the microfluidic chip containing 3D blood microvessels composed of human ECs and mesenchymal cells demonstrated superior binding ability of the Col IV-NPs to basement membrane after detachment of ECs by ammonium hydroxide treatment (*Figure 1C and D*). In particular, while Col IV-NPs strictly adhered to denuded walls (arrows in *Figure 1C*, middle panel), indicating firm adhesion of Col IV-NPs to their target; bare NPs mainly diffused within the tubules without adhering to the basement membrane (arrows in *Figure 1C*, right panel). DsRed-labelled ECs (in red) and immunostained Col IV (in green) in *Figure 1D* qualitatively reveals the efficiency of EC removal after ammonium hydroxide treatment and shows Col IV-NP co-localization with Col IV expressed in the basement membrane.

Col IV-targeting nanoparticles localize at the site of denuded intima *in vivo* and increase payload accumulation

After testing the adhesion properties of Col IV-NPs *in vitro* both in a 2D and 3D setting, we then investigated their targeting properties *in vivo* in an experimental mouse preparation of arterial intimal injury that recapitulates features of superficial erosion.[22] Briefly, 8-week-old ApoE$^{-/-}$ mice that consumed a normal chow diet underwent electrical injury of the LCCA using a bipolar microcoagulator (Erbe ICC 200, USA) as previously described.[22] Twenty-eight days later, a neointima formed that replicated characteristics of human plaques complicated by erosion. We then induced local flow disturbance in proximity of the healed injury by placing perivascular constrictive polyethylene cuffs. This flow perturbation at the site of arterial neointima induces EC activation, apoptosis, and desquamation, uncovering the basement membrane (shown by black dashed line) exposed, processes implicated in superficial erosion (*Figure 2A*). This intervention resulted in neutrophil recruitment, activation, and degranulation, with subsequent NET release, which amplified and propagated the local inflammation.[22]

At 1 h after constrictive cuff placement, we tested the ability of injected rhodamine-labelled Col IV-NPs vs. bare NPs to target lesions that recapitulate features of superficial erosion. *Ex vivo* fluorescence analysis of NP accumulation in both LCCA (injured) and right common

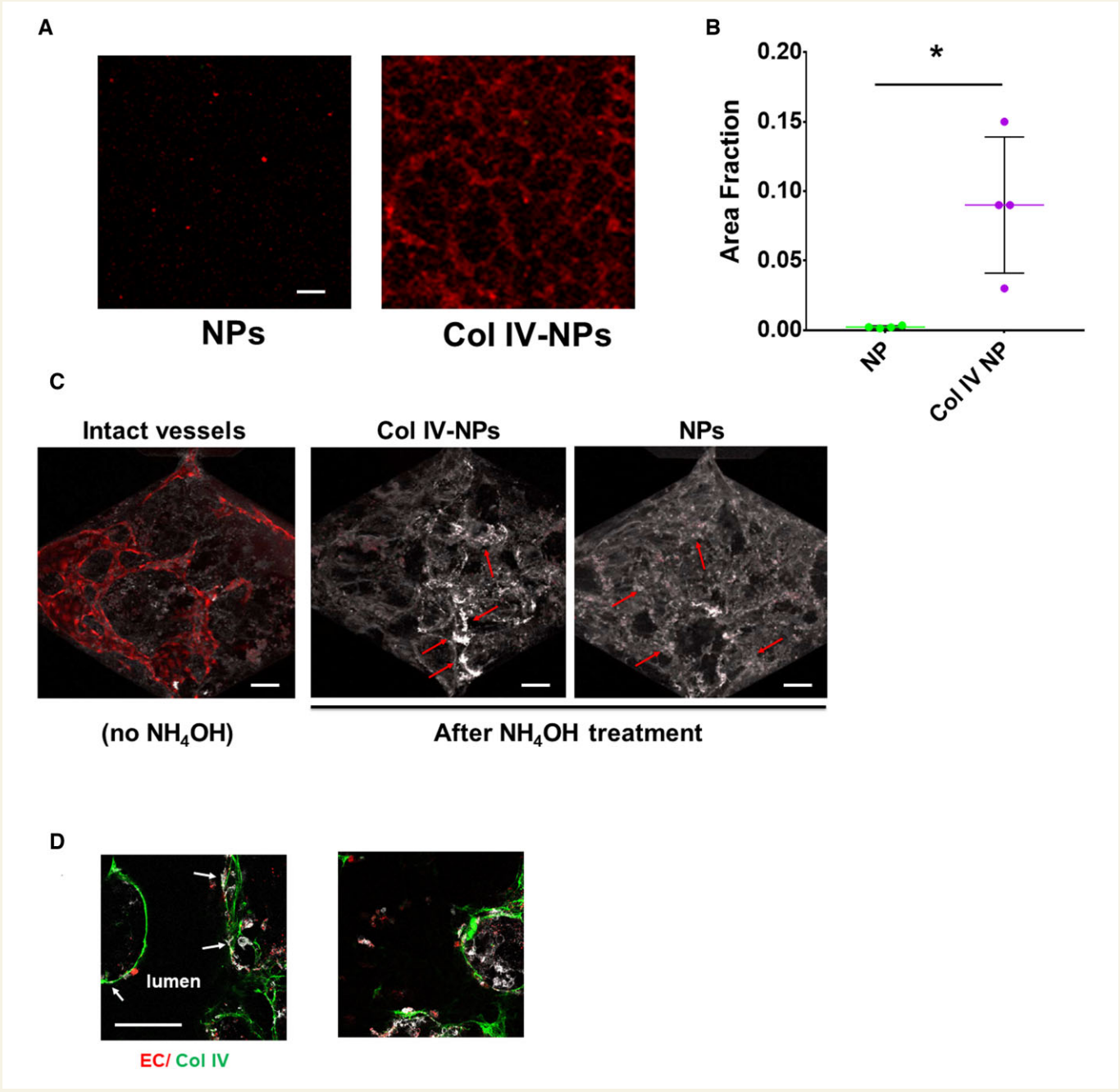

Figure 1 Collagen IV-targeting nanoparticles adhere *in vitro* to basement membrane produced by endothelial cells in both 2D and 3D settings. (*A* and *B*) Compared to non-targeting NPs, Col IV-NPs showed 40-fold increased adhesion to HSVEC-produced basement membrane on a glass slide ($n = 4$). (scale bar = 100 μm) (*C*) When tested in a 3D setting, we observed a tubule-shaped binding for Col IV-NPs and a more diffuse deposition for the non-targeting NPs (red arrows). (*D*) DsRed-labelled ECs (in red), Col IV (in green), and Col IV-NPs (in white) reveals co-localization of NPs at sites of exposed Col IV after EC removal. Mann–Whitney test. $^*P < 0.05$.

carotid artery (RCCA) (control) at 24 h after NP administration revealed a significantly higher accumulation of Col IV-NPs compared to bare NPs (1.8-fold increase, $P < 0.0001$) (*Figure 2B and C*). In addition, analysis of both downstream and upstream fluorescent signals showed a preferential accumulation of Col IV-NPs downstream of the injury, while bare NPs showed no significant difference (Supplementary material online, *Figure S2*). Immunofluorescence investigation of NP localization downstream of the injury revealed a differential accumulation of bare vs. Col IV-NPs. While untargeted particles localized around the adventitia, the artery's outer layer, Col IV-NPs adhered from the luminal side to areas of denuded endothelium (white arrows in *Figure 2D*, middle panels). In addition, Col IV staining using an anti-Col IV antibody revealed colocalization with the targeted but not the bare NPs, thus delineating the effective targeting capabilities provided by the heptapeptide (*Figure 2E*). On the contrary, Col IV-NPs did not accumulate on the RCCA (Supplementary material online, *Figure S3*). For comparison, Supplementary material

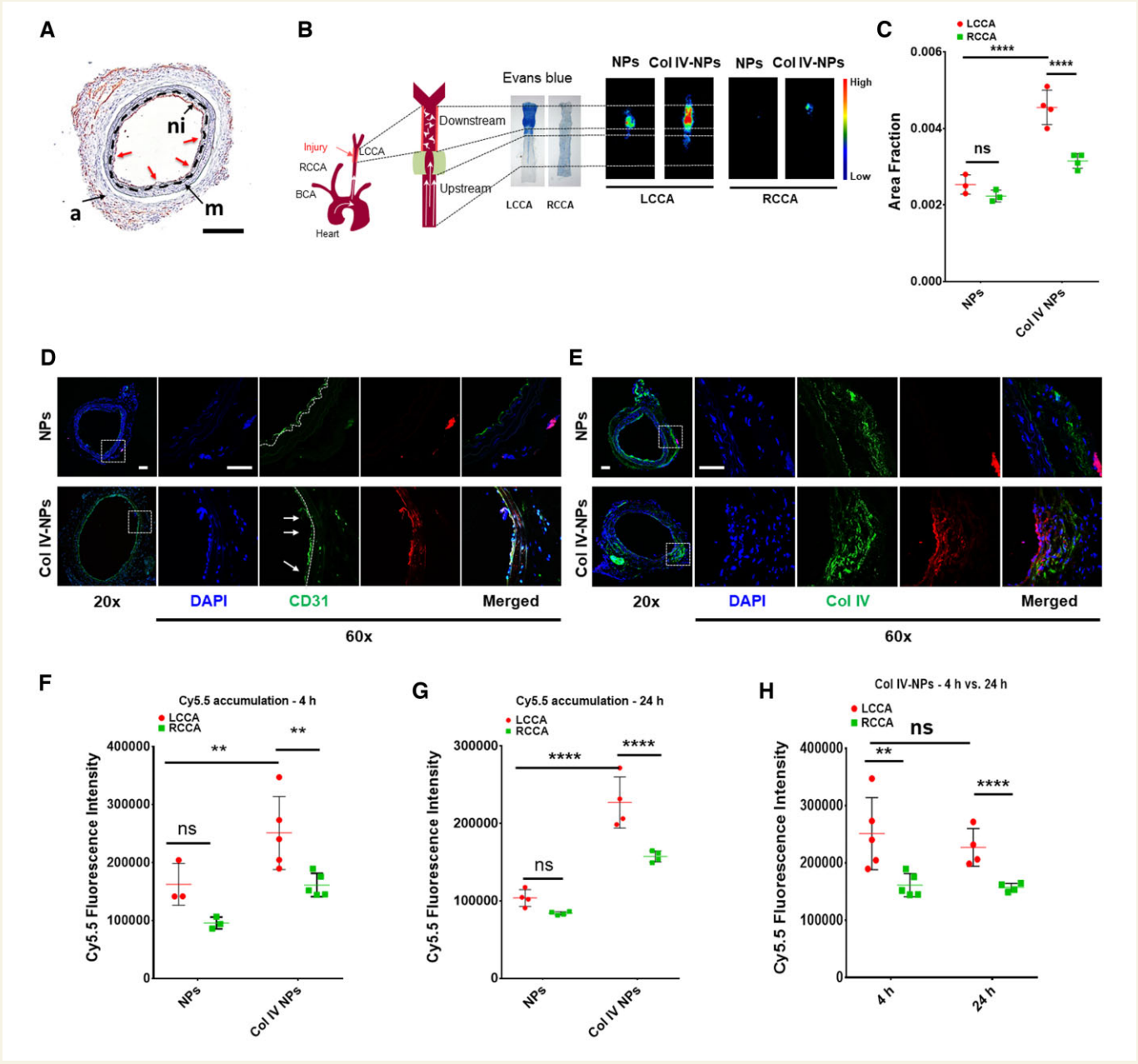

Figure 2 *In vivo* targeting of Col IV to exposed basement membrane after induction of flow disturbance to recapitulate aspects of superficial erosion. (*A*) Immunohistochemical analysis of *in vivo* preparation of superficial erosion in mice. Microscopic observation reveals neo-intima formation (ni) and areas of denuded endothelium (red arrows) and exposed basement membrane (black dashed line). (Scale bar 100 µm). (*B*) A constrictive cuff was placed on previously injured and healed LCCA to perturb flow. Representative Evans Blue staining reveals increased endothelial permeability in areas of disturbed flow. Fluorescence reflectance images of RCCA (healthy carotid) and LCCA ('eroded' plaque) in mice injected with bare NPs and Col IV-NPs at 24h post-injection. (*C*) Quantitative assessment of fluorescence intensities of bare and Col IV-NPs reveals a 1.8-fold higher accumulation for Col IV-NPs to denuded endothelium compared to bare NPs ($n = 3–4$). (*D* and *E*) Immunofluorescent staining of CD31 (*D*) and Col IV (*E*) shows NP localization downstream of the flow perturbation. Col IV-NPs co-localize with areas of desquamation (white arrows in *D*) and rich in Col IV (*E*). (Scale bar = 25 µm). (*F–H*) Quantitative assessment of fluorescence intensities using fluorescence reflectance imaging analysis of bare or Col IV-NPs loaded with cy5.5 shows higher payload accumulation when delivered by Col IV-NPs at both 4 and 24 h after injection ($n = 3–5$): Tukey's multiple comparisons test: $^{**}P < 0.01$; $^{****}P < 0.0001$.

online, *Figure S3* (middle panel, CD31) shows a control healthy artery with an intact endothelium. En face fluorescent visualization of cy5.5-labelled NPs validated the immunofluorescence results, revealing an increased accumulation of Col IV-NPs in areas corresponding to intimal denudation (Supplementary material online, *Figure S4*).

We further investigated the ability of the targeted NPs to deliver a payload selectively. As a proof of concept, we encapsulated

cyanine—an indicator small molecule—into bare and Col IV-NPs, and evaluated their accumulation to the target tissue 4 and 24 h after their systemic administration. Fluorescence evaluation from the fluorescence reflectance imaging analysis of harvested carotids indicated a substantially enhanced accumulation in regions of eroded plaques in mice that bear such lesions compared to control NPs at both 4 ($P < 0.01$) and 24 h ($P < 0.0001$) (*Figure 2F and G*). In addition, the payload remained within the lesion for at least 24 h (*Figure 2H*). These findings prompted *in vivo* study in mice of the ability of a nanoparticle-delivered PAD4 inhibitor to limit local NET formation at sites of endothelial disturbance.

Targeted local administration of the small molecule PAD4 inhibitor GSK484 reduces NET release *in vivo*

Having assessed the physicochemical and targeting properties of Col IV-NPs, we then tested the therapeutic efficacy of NPs that incorporated the PAD-4 inhibitor GSK484 (GSK) in mice with experimental superficial erosion. GSK encapsulation within Col IV-NPs slightly increased their average diameter, as revealed by DLS analysis (*Figure 3A*). Indeed, compared to empty Col IV-NPs (hydrodynamic size of empty Col IV-NPs = 65.3 nm; PDI = 0.24), GSK encapsulation induced an increase of the hydrodynamic size of about 30 nm (hydrodynamic size of GSK-loaded Col IV-NPs 94.6 nm), while drug loading did not significantly alter size distribution (PDI = 0.23) and surface charge, which was around -12 mV for both empty and GSK-loaded Collagen IV-targeted nanoparticles (Col IV NPs) (*Figure 3A and B*). We observed a similar trend for both empty and GSK-loaded bare NPs in terms of hydrodynamic size, size distribution and surface charge (Supplementary material online, *Figure S5*). TEM analysis validated DLS results and revealed a spherical morphology for both GSK-loaded NPs (*Figure 3C*). The encapsulation efficiency of GSK into Col IV-NPs was 55% of the initial amount, equivalent to a loading amount of 2.8% by weight. Kinetic studies showed slow release of GSK, which reached around 70% at 3 days (*Figure 3D*).

We then tested the uptake of Col IV-NPs by neutrophils isolated from mouse blood, which had adhered to the basement membrane deposited by HSVECs using the conditions described above for the *in vitro* adhesion studies. Co-localization experiments of fluorescently labelled NPs and neutrophils revealed internalization of both bare and Col IV-NPs (*Figure 4A and B*). Targeting experiments *in vivo* validated the *in vitro* results. After administration to mice with experimental superficial erosion, Col IV-NPs targeted the Col IV on denuded areas (*Figure 2E*) and co-localized with activated neutrophils (*Figure 4C*).

This finding engendered the hypothesis that PAD4 inhibition alleviates EC injury in experimental superficial erosion. We administered GSK, both free (4 mg/kg, once per day for 7 days) and encapsulated (4 mg/kg, three times in 7 days) into NPs, and evaluated the ability of its delivery to reduce NET accumulation at the site of denuded endothelium, to preserve endothelial continuity, and limit local neutrophil accumulation. At 7 days after treatment, both carotids were harvested for immunohistochemical and endothelial permeability analyses. The measurement of the LCCA neo-intimal area affirms the reproducibility of the surgical procedure, as well as the consistency of the injury among the groups (Supplementary material online, *Figure S6*). While free GSK did not significantly affect endothelial continuity, the treatment with Col IV-NPs protected ECs downstream of the flow disturbance against denudation (a four-fold increase in endothelial continuity percentage for Col IV NP-encapsulated GSK compared to free GSK, $P < 0.001$) (*Figure 5*) and reduced the amount of intimal NETs (a 2.5-fold reduction for the group treated with GSK-loaded Col-IV NPs vs. free GSK, $P < 0.01$) (*Figure 5*). Neither treatment altered neutrophil recruitment in the region of experimental superficial erosion (Supplementary material online, *Figure S7*). Endothelial permeability assessed by Evans Blue extravasation revealed that GSK-Col IV NPs preserved intimal barrier function in regions of flow perturbation significantly better that the other treatment groups ($P < 0.01$ vs. free GSK; $P < 0.0001$ vs. GSK-NPs) and to the untreated control ($P < 0.05$) (Supplementary material online, *Figure S8*). Encapsulation of GSK within Col IV-NPs provided better endothelial protection than free GSK or GSK loaded into non-targeted NPs, supporting the efficacy of this strategy for targeted delivery of a therapeutic payload.

Discussion

To date, the bulk of experimental investigations of ACS have focused on plaque rupture, a well-understood mechanism that is currently on the wane in an era of mastery over elevated low-density lipoprotein. This study used targeted delivery of an agent that inhibits NET formation to probe the mechanisms and explore a novel therapeutic approach using a recently validated mouse preparation that mimics features of human plaque erosion. We tested Col IV-NPs' adhesion properties both *in vitro* towards basement membrane naturally deposited by HSVECs and *in vivo* in a mouse preparation that recapitulates features of superficial erosion. *In vitro* experiments revealed that a ligand density of 15% conferred to Col IV-NPs the highest binding affinity, thus allowing them a 40-fold increased adhesion to the EC-derived basement membrane when compared to bare NPs (*Figure 1A and B*). In addition, when tested in a 3D setting, Col IV-NPs firmly adhered to denuded tubules while bare NPs diffused through them without adhering (*Figure 1C*). *In vivo* experiments showed that Col IV-NPs selectively targeted denuded regions downstream of flow disturbance induced by constrictive cuff placement in arteries with a tailored neointima. Immunofluorescence investigation showed luminal NP localization in areas of exposed basement membrane, while non-targeted NPs localized in the adventitia. The targeted release of the PAD4 inhibitor GSK by Col IV-NPs improved endothelial continuity and reduced NET accumulation at sites of intimal lesions compared to either free systemically-administered GSK or GSK-NP treatments (*Graphical abstract*). Evans Blue extravasation assay validated IHC results and confirmed a protective effect of GSK-Col IV NPs towards the endothelial barrier function in regions of superficial erosion.

These data provide further support for the participation of neutrophils and PAD4 in superficial erosion. This study also illustrated a novel approach to use targeted NP therapeutics to disrupt NETosis locally with high drug loading capacity, lesion-targeting capabilities, and tunable controlled release properties as potential tool to solve a heretofore largely neglected critical medical problem of growing clinical importance.

This study offers several points of interest: first, from a mechanistic standpoint, it extends current knowledge regarding the involvement of NETosis in aggravating endothelial injury related to superficial erosion. Moreover, from a pharmaceutical standpoint, basement membrane targeting through Col IV binding may furnish a diagnostic as well as a therapeutic tool. Indeed, in the context of superficial erosion, Col

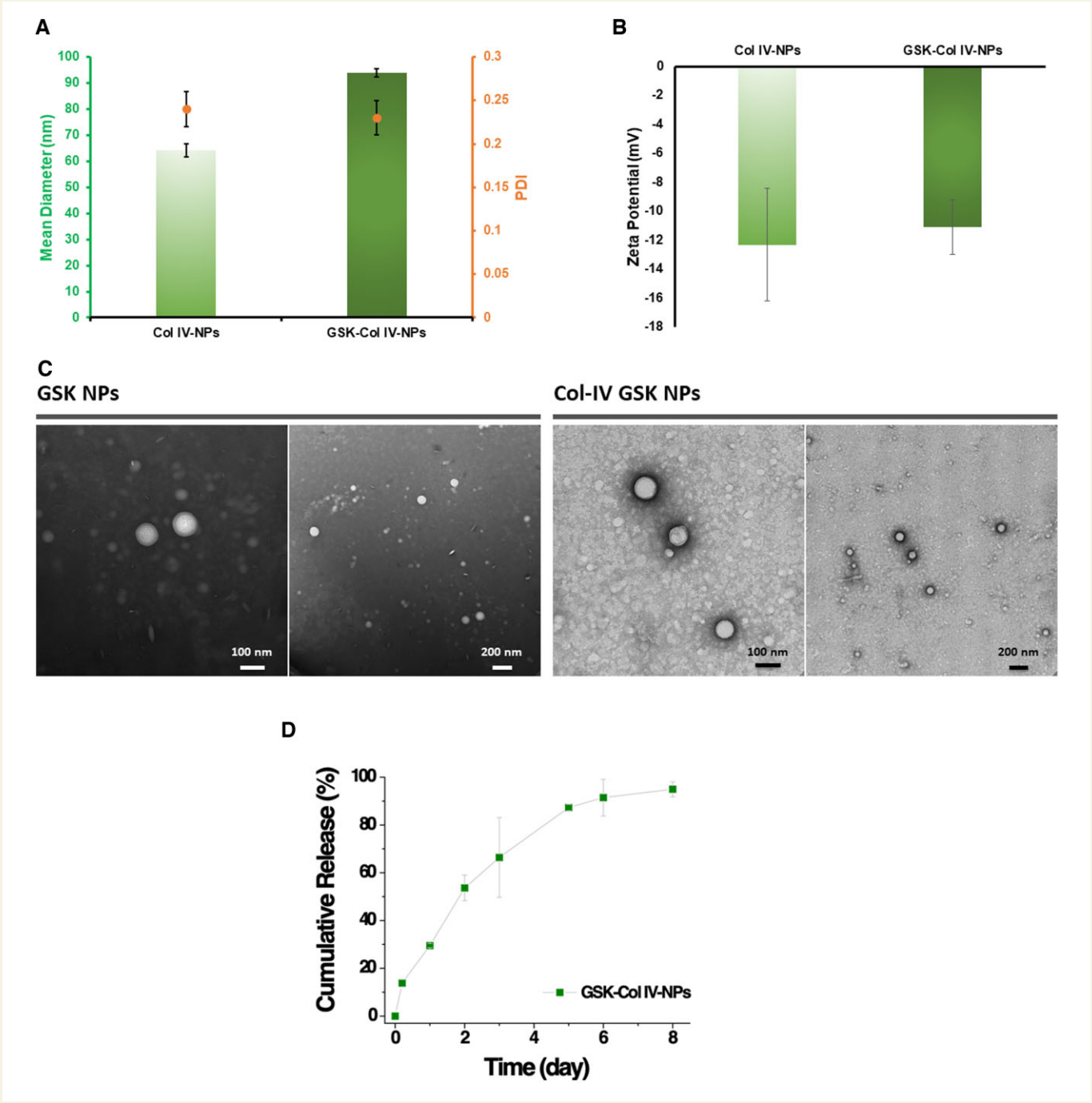

Figure 3 Physicochemical characterization of Col IV-targeting NPs. (*A*) Dynamic light scattering (DLS) analysis of empty and GSK484 (GSK)-loaded Col IV-NPs reveals a slight increase of the hydrodynamic size after GSK encapsulation (64 and 94 nm for empty and GSK Col IV-NPs, respectively). GSK encapsulation did not significantly affect the homogeneity of the formulations, as indicated by the polydispersity index values before and after GSK encapsulation (PDI = 0.24 and 0.23, respectively). (*B*) Zeta potential analysis reveals a negative surface charge for both empty and GSK-loaded Col IV-NPs, without significant changes after GSK encapsulation. (*C*) Representative TEM images of GSK NPs and Col IV GSK NPs validates DLS analysis. (*D*) Cumulative release of GSK from Col IV NPs at 37°C.

IV PLGA nanoparticles could localize to the basement membrane at early stages of erosion development, while not targeting stable lesions with an intact endothelium. Such nanoparticles could not only carry a therapeutic payload, but could contain an imaging agent, an example of a theranostic agent. The versatility in formulation of polymeric nanoparticles renders them able to carry various imaging beacons, i.e. fluorescent, PET, near-IR, MRI. This approach could provide a tool for non-invasive diagnosis of superficial erosion, a point of potential

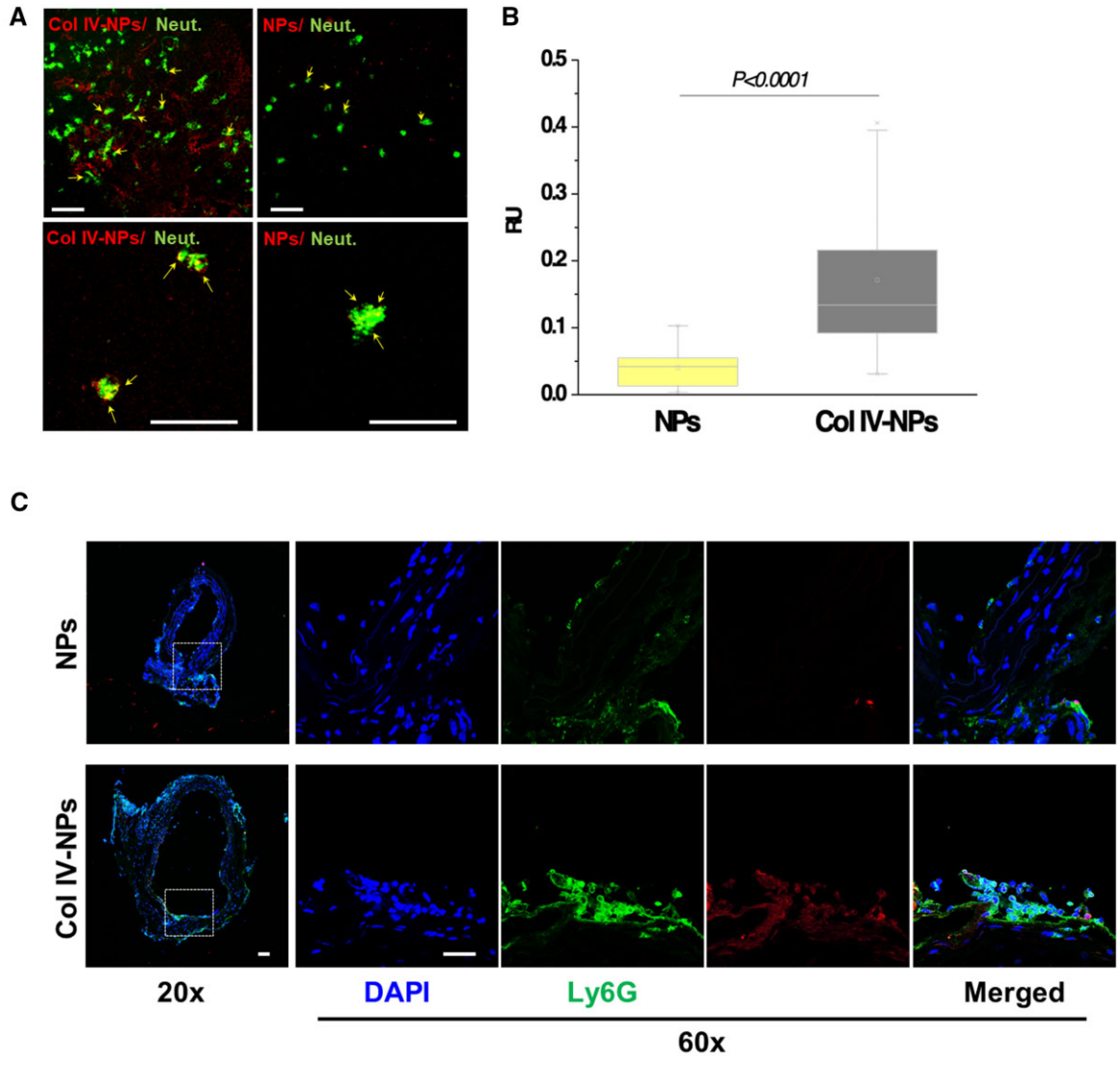

Figure 4 *In vitro* evaluation of Col IV-NPs targeting to basement membrane. (*A*) Confocal images of bare and Col IV-NPs (in red) incubated with primary mouse neutrophils (in green) in conditions that mimic superficial erosion. Arrows show NPs internalized in neutrophils (scale bar = 100 μm). (*B*) Quantitative assessment of NP/neutrophil fluorescent co-localization ($n = 24$ per group). (*C*) Immunofluorescent staining of Ly6G (neutrophil marker—in green) shows NPs localization downstream of the flow perturbation. Col IV-NPs co-localize with neutrophils recruited at areas of exposed basement membrane recapitulating eroded plaques. (Scale bar = 25 μm). Mann–Whitney test. $P < 0.0001$.

clinical relevance.[24] This approach clearly requires considerable development before human application. Many steps, from scalable manufacturing to regulatory, require consideration before clinical translation of this strategy.

From a therapeutic standpoint, instead, such adjunctive therapy should permit less intense antiplatelet therapy, for example omitting the upfront administration of glycoprotein IIb/IIIa inhibitors used in many patients in the EROSION study, thus reducing the risk of bleeding complications.[24] Thus, the present results both augment pathophysiologic insight into superficial erosion as a cause of ACS and illustrate a novel potential therapeutic intervention for this relatively neglected driver of arterial thrombosis.

Supplementary material

Supplementary material is available at *Cardiovascular Research* online.

Authors' contributions

Substantial contributions to the conception or design of the work (R.M., M.Y., P.L., O.C.F., J.S.); or the acquisition, analysis, or interpretation of data for the work (R.M., C.C., E.J.F., C.A.B., G.Y.L., Y.T., E.S., G.K.S., F.K., K.J.C., G.S., Y.L.). Drafting the work or revising it critically for important intellectual content (R.M., M.Y., P.L., G.K.S., C.A.B.). Final approval of the version to be published (all authors). Agreement to be accountable for

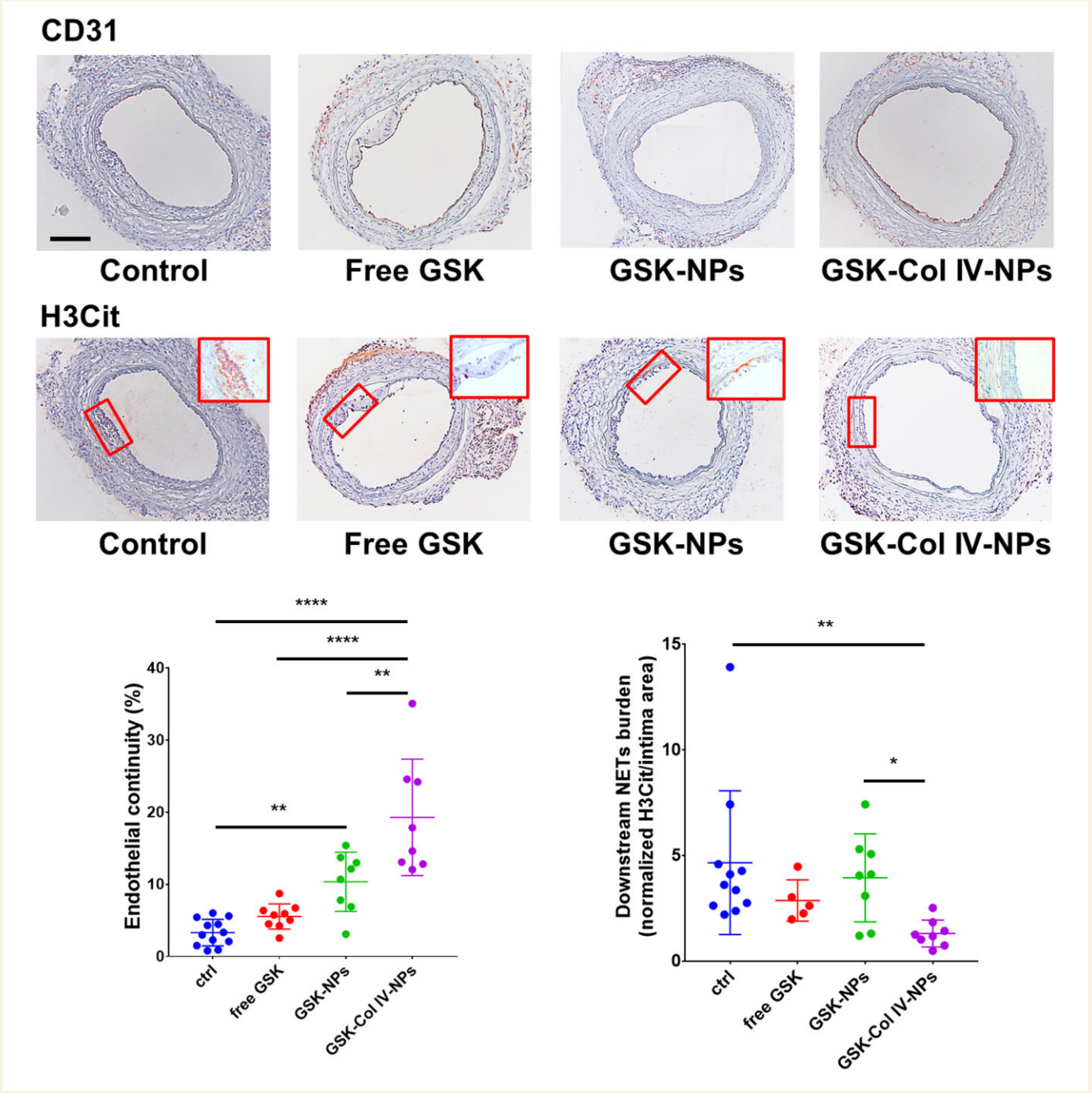

Figure 5 Therapeutic efficacy of GSK484-loaded Col IV-targeted NPs in a mouse preparation of superficial erosion. Immunohistochemical analysis of previously injured LCCA subjected to flow perturbation from mice ($n = 8$–12 per group, representative image shown) treated with free GSK484 (GSK) and GSK-loaded into bare NPs (GSK-NPs) and Col IV-NPs (GSK-Col IV-NPs). NPs were injected in PBS as vehicle. CD31 (endothelial cell marker) and H3Cit (citrullinated histone, neutrophil extracellular traps marker) staining revealed a significantly improved therapeutic efficacy for the group treated with GSK-Col IV-NPs as gauged by preservation of endothelial continuity and reduction of NET accumulation downstream of the flow perturbation, as shown by the representative data in the graph. Inserts show higher magnification of H3cit staining. (Scale bar 100 μm). One-Way ANOVA. *$P < 0.05$; **$P < 0.01$; ****$P < 0.0001$.

all aspects of the work in ensuring that questions related to the accuracy or integrity of any part of the work are appropriately investigated and resolved (all authors).

Conflict of interest: P.L. is an unpaid consultant to, or involved in clinical trials for Amgen, AstraZeneca, Esperion Therapeutics, Ionis Pharmaceuticals, Kowa Pharmaceuticals, Novartis, Pfizer, Sanofi-Regeneron, and XBiotech, Inc. P.L. is a member of scientific advisory board for Amgen, Corvidia Therapeutics, DalCor Pharmaceuticals, IFM Therapeutics, Kowa Pharmaceuticals, Olatec Therapeutics, Medimmune, Novartis, and XBiotech, Inc. P.L.'s laboratory has received research funding in the last 2 years from Novartis. Dr. Libby's laboratory has received

research funding in the last 2 years from Novartis. Dr. Libby is on the Board of Directors of XBiotech, Inc. Dr. Libby has a financial interest in Xbiotech, a company developing therapeutic human antibodies. Dr. Libby's interests were reviewed and are managed by Brigham and Women's Hospital and Partners HealthCare in accordance with their conflict of interest policies. K.C. reports relationships to Abbott, Philips, Cardiovascular Systems, Inc., and Abiomed. O.C.F. declares financial interests in Selecta Biosciences, Tarveda Therapeutics, Placon Therapeutics, and Seer.

Funding

R.M. is supported by the American Heart Association (18CSA34080399) and a generous gift from the RRM Fund. M.Y. is supported by the American Heart Association (18CSA34080399). G.S. is supported by the Lemann Foundation Cardiovascular Research Postdoctoral Fellowship Harvard University/ Brigham and Women's Hospital. C.B. is supported by the National Heart, Lung, and Blood Institute (R01 HL127030) and the Swiss National Science Foundation (SNSF) Postdoc Mobility Grant. PL receives funding support from the National Heart, Lung, and Blood Institute (R01HL080472 and 1R01HL134892), the American Heart Association (18CSA34080399), and the RRM Charitable and Simard Funds. O.C.F. and J.S. are supported by the American Heart Association (18CSA34080399).

Data availability

The data underlying this article will be shared on reasonable request to the corresponding author.

References

1. Stone GW, Maehara A, Lansky AJ, de Bruyne B, Cristea E, Mintz GS, Mehran R, McPherson J, Farhat N, Marso SP, Parise H, Templin B, White R, Zhang Z, Serruys PW; PROSPECT Investigators. A prospective natural-history study of coronary atherosclerosis. *N Engl J Med* 2011;**364**:226–235.
2. Pasterkamp G, den Ruijter HM, Libby P. Temporal shifts in clinical presentation and underlying mechanisms of atherosclerotic disease. *Nat Rev Cardiol* 2017;**14**:21–29.
3. Libby P, Pasterkamp G. Requiem for the 'vulnerable plaque'. *Eur Heart J* 2015;**36**: 2984–2987.
4. Tricot O, Mallat Z, Heymes C, Belmin JL, Lesèche G, Tedgui A. Relation between endothelial cell apoptosis and blood flow direction in human atherosclerotic plaques. *Circulation* 2000;**101**:2450–2453.
5. de Bont CM, Boelens WC, Pruijn GJM. NETosis, complement, and coagulation: a triangular relationship. *Cell Mol Immunol* 2019;**16**:19–27.
6. Yipp BG, Kubes P. NETosis: how vital is it? *Blood* 2013;**122**:2784–2794.
7. Lewis HD, Liddle J, Coote JE, Atkinson SJ, Barker MD, Bax BD, Bicker KL, Bingham RP, Campbell M, Chen YH, Chung CW, Craggs PD, Davis RP, Eberhard D, Joberty G, Lind KE, Locke K, Maller C, Martinod K, Patten C, Polyakova O, Rise CE, Rudiger M, Sheppard RJ, Slade DJ, Thomas P, Thorpe J, Yao G, Drewes G, Wagner DD, Thompson PR, Prinjha RK, Wilson DM. Inhibition of PAD4 activity is sufficient to disrupt mouse and human NET formation. *Nat Chem Biol* 2015;**11**:189–191.
8. Rohrbach AS, Slade DJ, Thompson PR, Mowen KA. Activation of PAD4 in NET formation. *Front Immunol* 2012;**3**:360.
9. Franck G, Mawson TL, Folco EJ, Molinaro R, Ruvkun V, Engelbertsen D, Liu X, Tesmenitsky Y, Shvartz E, Sukhova GK, Michel J-B, Nicoletti A, Lichtman AH, Wagner D, Croce KJ, Libby P. Roles of PAD4 and NETosis in experimental atherosclerosis and arterial injury: implications for superficial erosion. *Circ Res* 2018;**123**:33–42.
10. Chan JM, Zhang L, Tong R, Ghosh D, Gao W, Liao G, Yuet KP, Gray D, Rhee JW, Cheng J, Golomb G, Libby P, Langer R, Farokhzad OC. Spatiotemporal controlled delivery of nanoparticles to injured vasculature. *Proc Natl Acad Sci USA* 2010;**107**: 2213–2218.
11. Choi WI, Kamaly N, Riol-Blanco L, Lee IH, Wu J, Swami A, Vilos C, Yameen B, Yu M, Shi J, Tabas I, von Andrian UH, Jon S, Farokhzad OC. A solvent-free thermosponge nanoparticle platform for efficient delivery of labile proteins. *Nano Lett* 2014;**14**:6449–6455.
12. Kamaly N, Fredman G, Subramanian M, Gadde S, Pesic A, Cheung L, Fayad ZA, Langer R, Tabas I, Farokhzad OC. Development and *in vivo* efficacy of targeted polymeric inflammation-resolving nanoparticles. *Proc Natl Acad Sci USA* 2013;**110**:6506–6511.
13. Fredman G, Kamaly N, Spolitu S, Milton J, Ghorpade D, Chiasson R, Kuriakose G, Perretti M, Farokzhad O, Tabas I. Targeted nanoparticles containing the proresolving peptide Ac2-26 protect against advanced atherosclerosis in hypercholesterolemic mice. *Sci Transl Med* 2015;**7**:275ra220.
14. Kamaly N, Fredman G, Fojas JJ, Subramanian M, Choi WI, Zepeda K, Vilos C, Yu M, Gadde S, Wu J, Milton J, Carvalho Leitao R, Rosa Fernandes L, Hasan M, Gao H, Nguyen V, Harris J, Tabas I, Farokhzad OC. Targeted interleukin-10 nanotherapeutics developed with a microfluidic chip enhance resolution of inflammation in advanced atherosclerosis. *ACS Nano* 2016;**10**:5280–5292.
15. Yu M, Amengual J, Menon A, Kamaly N, Zhou F, Xu X, Saw PE, Lee SJ, Si K, Ortega CA, Choi WI, Lee IH, Bdour Y, Shi J, Mahmoudi M, Jon S, Fisher EA, Farokhzad OC. Targeted nanotherapeutics encapsulating liver X receptor agonist GW3965 enhance antiatherogenic effects without adverse effects on hepatic lipid metabolism in Ldlr(-/-) mice. *Adv Healthc Mater* 2017;**6**:10.1002/adhm.201700313.
16. Xu X, Saw PE, Tao W, Li Y, Ji X, Yu M, Mahmoudi M, Rasmussen J, Ayyash D, Zhou Y, Farokhzad OC, Shi J. Tumor microenvironment-responsive multistaged nanoplatform for systemic RNAi and cancer therapy. *Nano Lett* 2017;**17**:4427–4435.
17. Xu X, Wu J, Liu Y, Yu M, Zhao L, Zhu X, Bhasin S, Li Q, Ha E, Shi J, Farokhzad OC. Ultra-pH-responsive and tumor-penetrating nanoplatform for targeted siRNA delivery with robust anti-cancer efficacy. *Angew Chem Int Ed Engl* 2016;**55**:7091–7094.
18. Cedervall J, Dragomir A, Saupe F, Zhang Y, Ärnlöv J, Larsson E, Dimberg A, Larsson A, Olsson A-K. Pharmacological targeting of peptidylarginine deiminase 4 prevents cancer-associated kidney injury in mice. *OncoImmunology* 2017;**6**:e1320009.
19. Beltrami-Moreira M, Vromman A, Sukhova GK, Folco EJ, Libby P. Redundancy of IL-1 isoform signaling and its implications for arterial remodeling. *PLoS One* 2016;**11**:e0152474.
20. Rajavashisth TB, Liao JK, Galis ZS, Tripathi S, Laufs U, Tripathi J, Chai NN, Xu XP, Jovinge S, Shah PK, Libby P. Inflammatory cytokines and oxidized low density lipoproteins increase endothelial cell expression of membrane type 1-matrix metalloproteinase. *J Biol Chem* 1999;**274**:11924–11929.
21. Libby P, Ordovas JM, Birinyi LK, Auger KR, Dinarello CA. Inducible interleukin-1 expression in human vascular smooth muscle cells. *J Clin Invest* 1986;**78**:1432–1438.
22. Franck G, Mawson T, Sausen G, Salinas M, Masson GS, Cole A, Beltrami-Moreira M, Chatzizisis Y, Quillard T, Tesmenitsky Y, Shvartz E, Sukhova GK, Swirski FK, Nahrendorf M, Aikawa E, Croce KJ, Libby P. Flow perturbation mediates neutrophil recruitment and potentiates endothelial injury via TLR2 in mice—implications for superficial erosion. *Circ Res* 2017;**121**:31–42.
23. Bichsel CA, Hall SR, Schmid RA, Guenat OT, Geiser T. Primary human lung pericytes support and stabilize *in vitro* perfusable microvessels. *Tissue Eng Part A* 2015;**21**:2166–2176.
24. Jia H, Dai J, Hou J, Xing L, Ma L, Liu H, Xu M, Yao Y, Hu S, Yamamoto E, Lee H, Zhang S, Yu B, Jang IK. Effective anti-thrombotic therapy without stenting: intravascular optical coherence tomography-based management in plaque erosion (the EROSION study). *Eur Heart J* 2017;**38**:792–800.

Translational perspective

We have implicated neutrophil extracellular traps (NETs) in superficial erosion, a growing cause of acute coronary syndromes (ACS) in the current era. The enzyme protein arginine deiminase (PAD)-4 permits NET formation. Here, we describe the development of nanotherapeutics targeted to type IV collagen, a major basement membrane protein, that delivers selectively a PAD-4 inhibitor payload to experimentally eroded plaques. Improved endothelial integrity with this treatment supports PAD-4's mechanistic contribution to erosive lesion evolution. Targeted PAD4 inhibition thus provides a promising approach to block local NET formation, and to limit the propagation of intimal injury and thrombosis during ACS.